

Experimental Assessment of Turbocharged Diesel Engine Transient Emissions during Acceleration, Load Change and Starting

C.D. Rakopoulos, A.M. Dimaratos, E.G. Giakoumis

School of Mechanical Engineering, National Technical University of Athens, Greece

M.S. Peckham

Cambustion Ltd., Cambridge, UK

Copyright © 2010 SAE International

ABSTRACT

The control of transient emissions from turbocharged diesel engines remains an important objective to manufacturers, since newly produced engines must meet the stringent criteria concerning exhaust emissions levels as dictated by the legislated Transient Cycles. In the present work, experimental tests are conducted on a medium-duty, turbocharged and after-cooled diesel engine in order to investigate the behavior and formation mechanism of nitric oxide (NO), smoke and combustion noise emissions under various transient operating schedules including acceleration, load change and starting. To this aim, a fully instrumented test bed was set up in order to record and research key engine and turbocharger variables during the transient events. The main parameters measured are nitric oxide concentration and smoke opacity (both using ultra-fast response analyzers) as well as combustion noise. Various other variables were monitored, such as in-cylinder pressure, engine speed, fuel pump rack position, boost pressure and turbocharger speed. The main focus of the experimental investigation was devoted to engine acceleration tests representative of automotive and truck applications, commencing from various engine speeds and loads. The experimental test pattern also included load increases and (cold and hot) startings. Analytical diagrams are provided to explain the behavior of exhaust emissions development in conjunction with turbocharger and governor/fuel pump response. Turbocharger lag was found to be the main cause for the emissions peak values observed during all transient events. During starting, the lack of air and its mismatch with fueling caused excessive black smoke, identified by the extremely high values of exhaust gas opacity.

INTRODUCTION

The turbocharged diesel engine is currently the preferred powertrain system in medium and medium-large unit applications (trucks, land traction, ship propulsion, electricity generation). Moreover, it continuously increases its share in the highly competitive automotive market. In fact, diesel-engined vehicles have already secured a market share that is on a par with gasoline-engined ones across much of the European Union, they are beginning to gain considerable attention in the US, and this trend is sure to continue [1,2]. The most attractive feature of the compression ignition engine is its excellent fuel efficiency which can surpass 40% in vehicular applications and even 50% in large, two-stroke units for marine propulsion or electricity generation. Consequently, vehicles equipped with diesel engines achieve much lower specific fuel consumption and reduced carbon dioxide emissions than their similarly-rated spark ignition counterparts over the entire operating range and for the whole vehicle lifetime.

Traditionally, the study of diesel engine operation has focused on the steady-state performance, with much lesser attention paid to the unsteady or, more accurately termed, transient operation. However, the majority of daily driving schedule involves transient conditions. In fact, only a very small portion of a vehicle's operating pattern is true steady-state, e.g., when cruising on a motorway. Unsurprisingly then, the experimental and modeling analysis of transient diesel engine operation has turned out to be an important objective to engine manufacturers, intensified by the fact that significant deviations are experienced when comparing instantaneous transient emissions with the respective quasi-steady ones [3-7]. In response to this, various legislative directives in the European Union, Japan and the US, have drawn the attention of manufacturers and researchers all over the world to the transient operation of diesel engines, in the form of Transient Cycles Certification for new vehicles [8,9].

The fundamental aspect of transient conditions lies in its operating discrepancies compared with steady-state operation (i.e., operation at the same engine speed and fuel pump rack position of the respective transient cycles). Whereas during (fully warmed-up) steady-state conditions, crankshaft rotational speed and fueling, hence all the other engine and turbocharger properties remain practically constant, during transient operation, both the engine speed and the amount of injected fuel change continuously. Consequently, the available exhaust gas energy varies, affecting turbine enthalpy drop and, through the turbocharger shaft torque balance, the air-supply and boost pressure to the engine cylinders are influenced. However, due to various dynamic, thermal and fluid delays in the system, mainly originating in the turbocharger principle of operation and its dynamic moment of inertia, combustion air-supply is delayed compared with fueling, eventually affecting torque build-up (driveability) and exhaust emissions [3].

Over the past years, the modeling and the experimental investigation of the thermodynamic and gas dynamic processes in diesel engines has intensively supported the study of engine transient operation [e.g. 3,6,10-15]. However, the vital issue of exhaust emissions has not been researched completely owing to the following two major issues:

- As regards the modeling approach, incorporation of exhaust emissions predictions into transient (filling and emptying) simulation codes, via two-zone or better still multi-zone models, would lead to high or even prohibitive computational times for the large number of engine cycles needed to be simulated. Moreover, a vast number of calibrated engine constants would have to be established for each sub-model developed, a tremendous task no doubt.
- As regards the experimental approach, transient operation requires highly complicated, sophisticated and costly experimental facilities to be accurately reproduced such as a fully automated test-bed with electronically controlled dynamometer, fast response exhaust gas analyzers and even dilution tunnels for the reproduction of Transient Cycles.

As a result, a relatively small number of experimental works have been conducted so far [e.g. 5,16-19], while simulation studies are even more scarce [20-22], with sometimes uncertain results. Unsurprisingly, alternative modeling approaches have been proposed for predicting diesel engine transient emissions, e.g. based on steady-state mapping and applying correction factors to account for transient discrepancies [23,24]; on the other hand, reconstruction techniques of the measured signal using conventional slow response analyzers have been deployed, either by mathematical signal processing [25,26] or by modeling the gas flow into the analyzer [27].

The goal of this paper is to fill an apparent gap in the literature by studying the engine transient response and investigating the component contributions. To this aim, extended experimental tests were conducted on a medium-duty, turbocharged and after-cooled, direct injection diesel engine with the use of ultra-fast response emissions measurement instrumentation.

Unlike previous research, the experimental investigation carried out included all three of the major transient operation cases encountered in the daily operation of automotive and truck diesel engines, namely acceleration, load change and (cold and hot) starting. Particularly as regards the latter, exhaust gases during cold starting have recently gained increased attention (see for example, the New European Driving Cycle, or the US FTP-75, where the emissions are sampled with the engine cold started) owing to their significant contribution to total emissions from diesel-engined vehicles. For example, it has been found that a diesel engine may emit up to seven times more particulate matter during cold operation than under warm conditions [28,29] coupled also to a prolonged period of unacceptable smoke emissions [30].

The experimental investigation carried out initially focused on the measurement of the two most influential diesel engine pollutant emissions, i.e., nitric oxide and smoke, using ultra-fast response analyzers particularly suited to transient measurements. Moreover, the analysis was extended to another important (but often neglected) emission, namely combustion noise. Diesel engine noise radiation gets more and more attention in recent years [31-33], since it is associated with the passengers' and pedestrians' discomfort. By including the measurement of noise in this investigation, it was made possible to derive some useful conclusions regarding potential common mechanisms of all three examined emissions.

The current paper is organized as follows: First, the experimental test bed installation is presented in detail, with the main focus on the pollutant and combustion noise measurement devices. A description of the procedure followed during the investigation as well as a tabulation of the tests conducted is given afterwards. The next section presents the results of the study separately for each case of transient operation and for each emission measured. The results are given in a series of diagrams illustrating the response of engine and turbocharger operating parameters, as well as pollutants and combustion noise emissions development. Wherever needed, ancillary diagrams are provided to highlight specific aspects and offer a better insight into the engine processes. Finally, the paper concludes with a brief summary and the basic results drawn from the experimental investigation.

EXPERIMENTAL TEST BED INSTALLATION

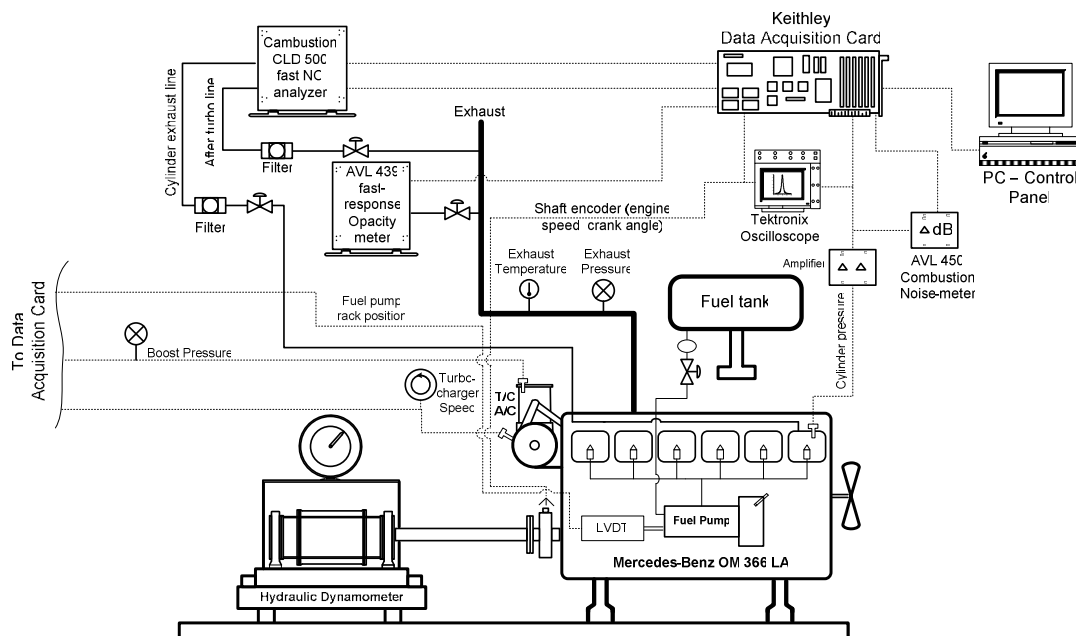


Figure 1. Schematic arrangement of the test bed installation, instrumentation and data acquisition system

A general layout of the test bed installation, the instrumentation used and the data acquisition system is illustrated in Figure 1. The description of the individual components will be detailed in the following subsections.

ENGINE UNDER STUDY

The engine used in this study is a Mercedes-Benz OM 366 LA, turbocharged and after-cooled direct injection diesel engine and is coupled to a hydraulic dynamometer of high moment of inertia. The specific engine is widely used to power mini-buses and small/medium trucks as for the Athens Urban Transport Organization; its basic technical data are given in Table 1. Two notable features of the engine are on the one hand its retarded fuel injection timing, in order to achieve low NO emissions, and on the other hand the fuel-limiter (cut-off) function. The latter is practically an aneroid device controlling the fuel pump rack maximum travel according to boost pressure in order to limit the exhaust smoke level during demanding conditions such as transients or low-speed, high-load steady-state operation. The engine is turbocharged with a fixed geometry Garrett turbocharger incorporating an internal waste-gate valve and an air-to-air after-cooler.

EMISSIONS MEASUREMENT

Fast NO Measurement

For the continuous measurement of NO emissions, the ultra-fast response analyzer CLD500 by Cambustion Ltd [34] is employed. It is a chemiluminescent detector used for measuring NO and NO_x (in the latter case incorporating a NO₂ to NO converter) concentration in the exhaust gas with a 90%-10% response time of approximately 2 ms for NO and 10 ms for NO_x [35,36]. This very short response time is achieved by locating the detectors in remote sample heads that are positioned very close to the sample point in the engine and conveying the sample gas to the detectors under the influence of a vacuum through narrow heated capillaries.

The operating principle of the CLD500 NO measurement is demonstrated in Figure 2. The complex reaction between NO and ozone (O₃) emits light; this reaction is the basis for the (very small) chemiluminescence detector (CLD) in which the photons produced are detected by a photo-multiplier tube located 10-metres down a fibre-optic bundle within the instrument's main control unit. The reaction chamber is coupled to a constant pressure sampling system in order to avoid exhaust sample pressure interference on the signal. The sample enters the reaction chamber through this constant pressure chamber. The CLD output voltage (signal) is proportional to NO concentration.

The CLD500 equipment has two remote sampling heads and is capable of simultaneous sampling at two different locations. For the current study, the two sampling positions are shown in Figure 1: one head is located exactly after the exhaust valve of cylinder No. 1 (this is the same cylinder from which the indicator diagrams were measured), capturing an individual cylinder's NO concentration, and the other head is located downstream of the turbocharger, capturing total NO emission concentration. Both heads are used during steady-state experiments, while during transient testing only the second sampling head was applied owing to data acquisition card limitations, as will be detailed later in the text.

After the experimental NO measurements were taken, the corrections required by the legislation have been carried out in order to convert the obtained values on a wet/dry basis.

Table 1. Engine and turbocharger specifications

Engine model and type		Mercedes Benz OM 366 LA, 6-cylinder, in-line, 4-stroke, compression ignition, direct injection, water-cooled, turbocharged, after-cooled, with bowl-in piston
Speed range		800–2600 rpm
Maximum power		177 kW @ 2600 rpm
Maximum torque		840 Nm @ 1250–1500 rpm
Engine total displacement		5958 cm ³
Bore / Stroke		97.5 / 133 mm
Connecting rod length		230 mm
Compression ratio		18:1
Firing order		1-5-3-6-2-4
Valve timings	Inlet valve opening	15° CA before TDC
	Inlet valve closure	25° CA after BDC
	Exhaust valve opening	68° CA before BDC
	Exhaust valve closure	12° CA after TDC
Fuel delivery system	Fuel pump	Bosch PE-S series, in-line, 6-cylinder with fuel limiter
	Governor	Mechanical, Bosch RQV 300/1300 MW157
	Injector body and nozzle	Bosch, 5 nozzles, opening pressure 250 bar
	Static injection timing	5±1°CA before TDC
Aspiration	Turbocharger model	Garrett TBP 418-1 with internal waste-gate
	Compressor	Single-stage, centrifugal
	Turbine	Fixed geometry, single-stage, twin-entry, radial
	After-cooler	Air-to-air

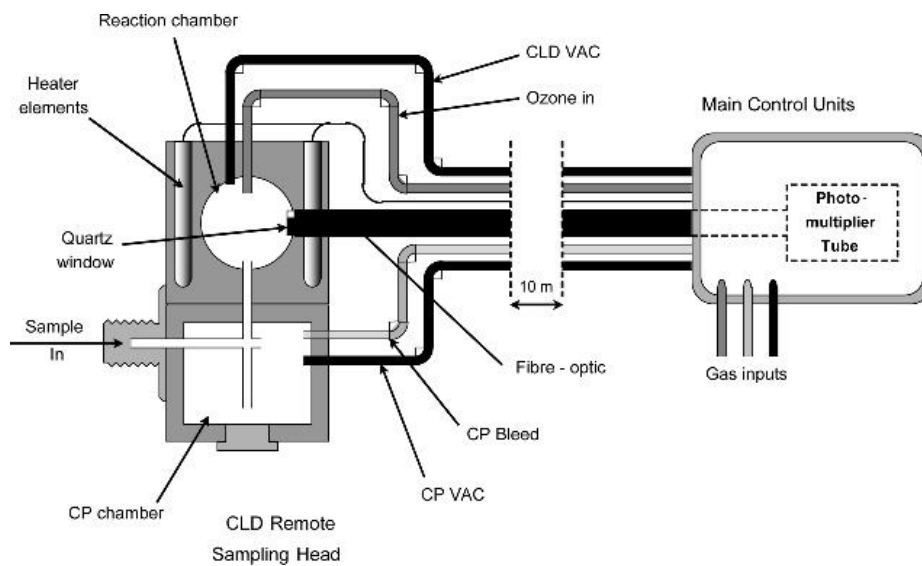


Figure 2. Schematic diagram of ultra-fast CLD500 operating principle (NO measurement)

Fast Opacity Measurement

The exhaust gas opacity is measured continuously with the AVL 439 partial flow Opacimeter. This is a device particularly suitable to transient measurements since the sample flows continuously through the opacimeter which has an analog output rate of 50 Hz. During the measurement, a constant sample of the exhaust gas is continuously extracted and guided to the measuring chamber, without prior dilution, through a conditioning tube heated at 100°C in order to prevent hydrocarbon condensation and particle deposition. The measuring chamber of the AVL 439 Opacimeter is of non-reflecting surface and has a length of 0.430 m, at the two ends of which the light source (halogen lamps) and the light detector unit are located. The opacity of the sample is determined from the measurement of the attenuation of visible light by the smoke in the exhaust gas sample located between the source and the detector unit [37]. Attenuation of light is caused by scattering by the particles and absorption in the particles. After exiting the measuring chamber, the gas sample is guided back to the exhaust pipe of the engine.

Opacimeter control is achieved using the AVL 4210 Instrument Controller through which all the opacimeter functions and parameter settings are selected. The opacimeter outputs the measurement either in terms of opacity (0–100%) or absorption coefficient ($0\text{--}10\text{ m}^{-1}$) in analogue or digital form, while various algorithms (floating mean, Bessel, 1st order low pass) can be selected to filter the signal. Its technical characteristics comply with the legal requirements such as ECE R24, SAE J 1667 and the ELR Test Cycle, with the respective filter algorithms preprogrammed into the opacimeter.

In this study, it is the analogue output that is used and the measurements are expressed in opacity values (%). No filter algorithm is applied ('raw' signal), in order successfully to capture all the smoke emission peaks. The location of sampling and return lines, as can be seen in Figure 1, is downstream of the turbocharger.

Combustion Noise Measurement

Combustion noise measurement is achieved using the AVL 450 Combustion Noise Meter. Its operating principle is based on the analysis of the indicator diagrams on the frequency domain applying a series of filters

to it [38]. Initially, the cylinder pressure signal passes through a U-filter, corresponding to the frequency attenuation of the engine block. Afterwards, there is a possibility of filtering combustion chamber resonance with selectable low-pass filters switchable on the front panel of the instrument, which, however, may induce measuring faults [38]. Finally, the signal is guided through an A-filter that matches a standard value correction in acoustics to the audible characteristics of the human ear. The produced output signal is further processed by RMS (root mean square) conversion to logarithmic DC values that relate to the aural threshold. The final output signal is given as a digital display in dB on the front panel of the instrument as well as an analogue voltage proportional to the combustion noise value. The former output is used during steady-state measurements, while the latter is selected during transient testing. In the current work, the combustion noise meter is placed after the cylinder pressure signal amplifier, as shown in Figure 1, and is operated without any low-pass filters.

MEASUREMENT OF ENGINE OPERATING PARAMETERS

The engine operating parameters measured and recorded continuously are: engine speed; cylinder pressure; fuel pump rack position; boost pressure and turbocharger speed. The location of each measuring device on the experimental test bed installation is given in Figure 1. A few details concerning the various measuring devices are provided below.

Engine Speed

The engine speed during each cycle is calculated using the signal of a Kistler shaft encoder. This signal is also used for time/crank angle reference.

Cylinder pressure

The instantaneous cylinder pressure measurement is performed using a Kistler miniature piezoelectric transducer, type 6051A, mounted on the cylinder head combined with a Kistler charge amplifier, type 5007. The cylinder pressure signal is continuously monitored on a dual beam Tektronix oscilloscope together with the shaft encoder signal.

Fuel pump rack position

The instantaneous position of the fuel pump rack is measured using a Linear Variable Differential Transducer (LVDT), type DC25, by Solartron Metrology. It is connected mechanically to the fuel pump rack and is capable of measuring displacements of ± 25 mm. A custom made 'stop' with various adjustable positions, each one corresponding to a specific engine speed, was fitted on the pedal in order to ensure constant pedal position at the end of each acceleration test as well as repeatability of the accelerations.

Boost pressure

Boost pressure is measured at two different locations, one immediately downstream of the turbocharger compressor, using a conventional manometer, and the second at the inlet manifold of the engine after the after-cooler. For the continuous measurement of boost pressure at the second location, a pressure transmitter manufactured by Wika, type A-10, is used.

Turbocharger speed

The measurement of turbocharger speed is achieved using a Garrett Turbo Speed Sensor. The sensor is placed on the compressor housing, which is drilled in the appropriate way, so that the sensor can 'see' both full and

splitter blades. The output signal is a square-wave one at 1/8th the input frequency. The latter is simply one pulse per blade, as the blades pass in front of the sensor. Taking into consideration the number of compressor wheel blades, the turbocharger speed can then be calculated. The output signal is recorded continuously, whereas a conventional analogue tachometer (speed gauge) is also employed for an initial estimation of the turbocharger rotational speed.

Exhaust pressures and temperatures at various locations were also measured during steady-state conditions with conventional analogue devices. Additionally, fuel consumption measurement was taken during steady-state operation with the use of a gravimetric fuel tank.

DATA ACQUISITION AND PROCESSING SYSTEM

All the above mentioned signals from the measuring devices and instruments are fed to the input of the data acquisition module, which is a Keithley KUSB 3102 ADC card connected to a Pentium Dual Core PC, via USB interface. This type of connection offers great flexibility and easiness in use, avoiding difficult electronic connections to the PC and special settings. The specific type has a maximum sampling rate of 100 ksamples/s, with a 12-bit resolution for its 8 differential analogue inputs. For the present study and during transient measurements these were 1: engine speed; 2: fuel pump rack position; 3: cylinder pressure; 4: turbocharger speed; 5: boost pressure; 6: combustion noise; 7: opacity and 8: NO emission. Also it possesses 2 output analogue channels, 17 digital input/output lines and 2 counter/timers. Control of this high-speed acquisition system is achieved by using the 'quickDAQ' data collecting software, supplied by Keithley together with the KUSB 3102 ADC card. Following the storage of the recorded measurements into files, the data are processed using an in-house developed computer code.

EXPERIMENTAL PROCEDURE

Various transient tests were carried out covering all three major cases of transient operation, i.e., acceleration, load change and starting, with the main focus being on the former, given that the engine is intended for automotive applications. Since the engine is coupled to a hydraulic dynamometer in all the cases where acceleration events are studied, the brake load also increases, which is actually the case when a vehicle accelerates (the increase in engine/vehicle speed results in an increase of both tire rolling and aerodynamic resistance). The engine was allowed to stabilize at the initial steady-state condition and then either the fuel pump rack was shifted to a greater fuel supply position to accelerate the engine (pedal pushed to the end of the adjustable custom made 'stop') or, for load changes, the brake load was (instantaneously) increased by moving the brake control lever under constant pedal position. The acceleration tests were performed for various combinations of initial rotational speeds and loads, mimicking vehicle real acceleration under different (vehicle) speed and gear; the details are given in Table 2. Figure 3 illustrates the initial and final conditions of the tests in a speed-load graph. The experimental study extended to the investigation of engine starting, under both cold and hot conditions. The key parameter used to determine the starting conditions was the coolant temperature; the pedal was fixed to a specific position corresponding to the desired engine idling speed and then the starter button was pushed.

Table 2. Tabulation of test conditions

Transient tests					
Type of test		Initial Conditions		Final Conditions	
		Speed (rpm)	Load (%)	Speed (rpm)	Load (%)
1.	Acceleration	1035	10	1670	12
2.	Acceleration	1035	10	2110	18
3.	Acceleration	1530	10	2080	20
4.	Acceleration	1530	40	2055	75
5.	Load Increase	2034	10	1202	50
Engine Starting Tests					
Conditions		Idling Speed (rpm)		Coolant Temperature (°C)	
6.	Cold	880		20	
7.	Hot	930		80	

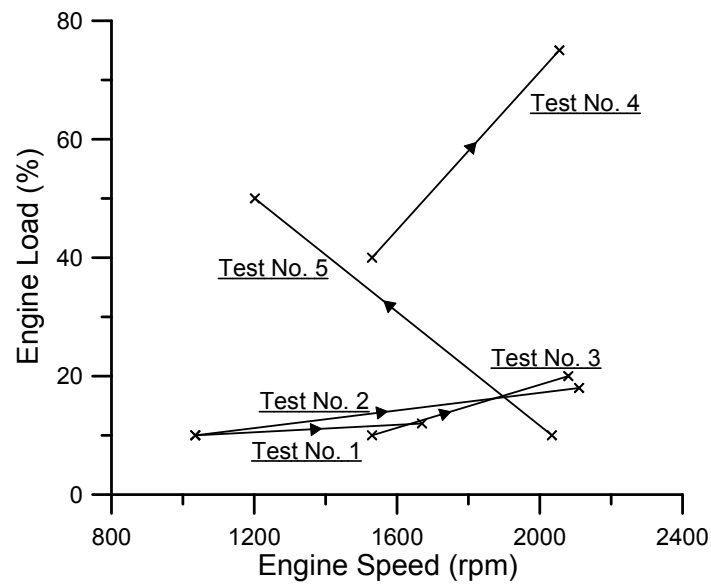


Figure 3. Initial-final conditions of each test

RESULTS AND DISCUSSION

ACCELERATION TESTS RESULTS

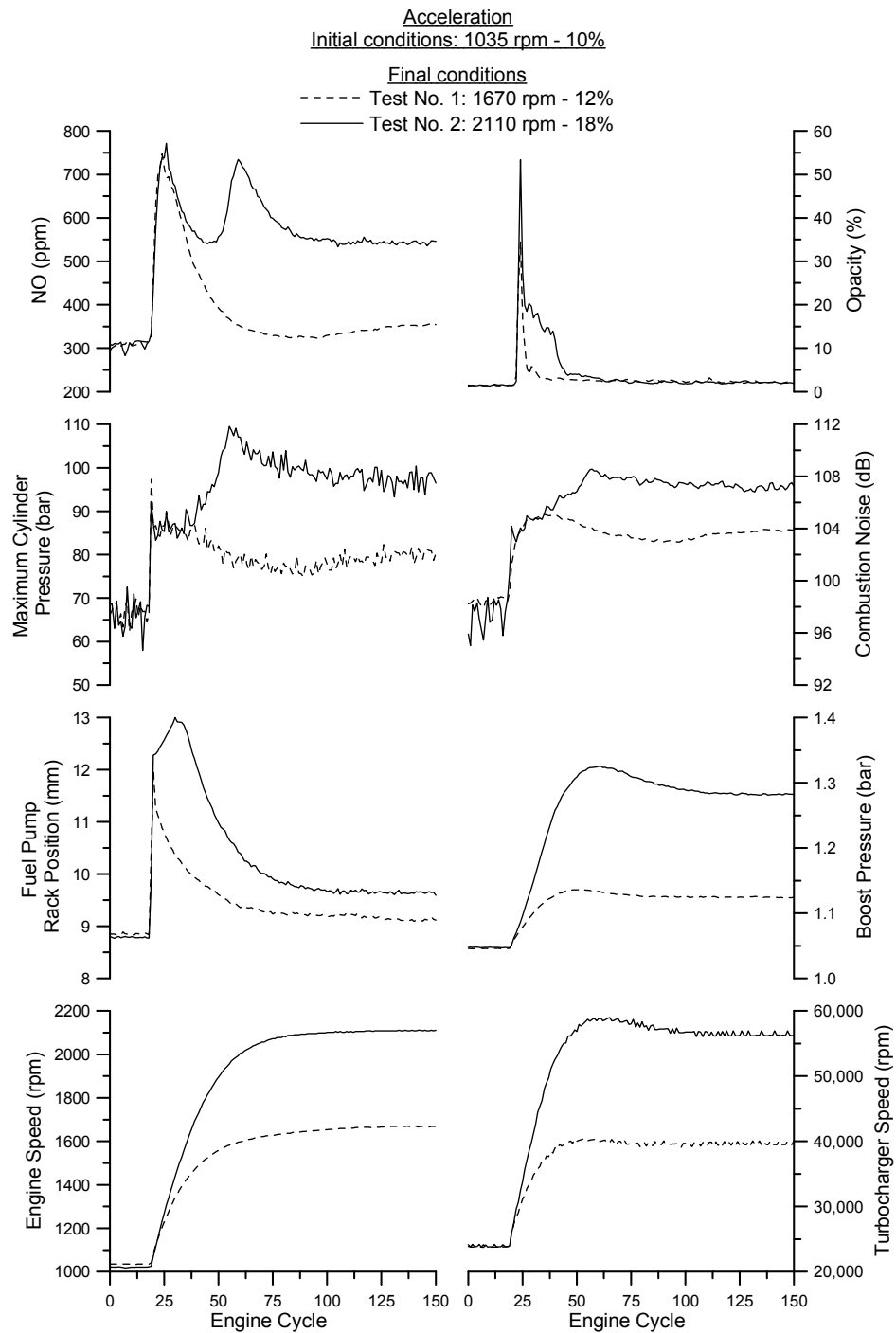


Figure 4. Development of engine and turbocharger variables and emissions response during two accelerations from low load

Figure 4 illustrates the results for the first two acceleration tests (No. 1 and No. 2 of Table 2) commencing from the same initial operating conditions, i.e., engine speed 1035 rpm and 10% load. This test represents vehicle acceleration from low gear. It is the final engine speed that varies between the two cases, with the brake loading following accordingly (since the brake connected to the engine is a hydraulic one, its torque rises with the second power of speed – the same applies for the aerodynamic resistance term for vehicular applications). The response of five engine and turbocharger operating parameters as well as the development of the three (pollutant and noise) emissions is demonstrated in this figure. For each case, the engine was allowed to settle at the initial steady-state conditions before the pedal was abruptly pushed (to its adjustable ‘stop’) to accelerate it. These two tests are particularly demanding for both the engine and the turbocharger, since the latter accelerates from practically zero boost.

As made obvious from Figure 4, the fuel pump rack responds almost instantly to the fueling increase command (with the injection pressure following a qualitatively similar development) and shifts to its maximum position, leading to higher fueling. Particularly during the most demanding test No. 2, the fuel pump rack responds in two stages; initially, a rapid shift to a first peak position is observed, followed by a smoother movement to the maximum position. The latter behavior highlights in the most explicit way the fuel limiter operating principle that does not allow sharp fueling increases when the boost pressure is still low. Indeed, boost pressure remains practically unchanged during the early transient cycles as can be further observed in Figure 5. Clearly, the increased exhaust gas power is not capable of instantly increasing the turbine power output, largely owing to the turbocharger inertia, so that the compressor operating point moves rather slowly towards the direction of increased boost pressure and air-mass flow-rate; during this period (12 engine cycles or 1.17 s), known as turbocharger lag, the engine is practically running in naturally aspirated mode or with very low boost.

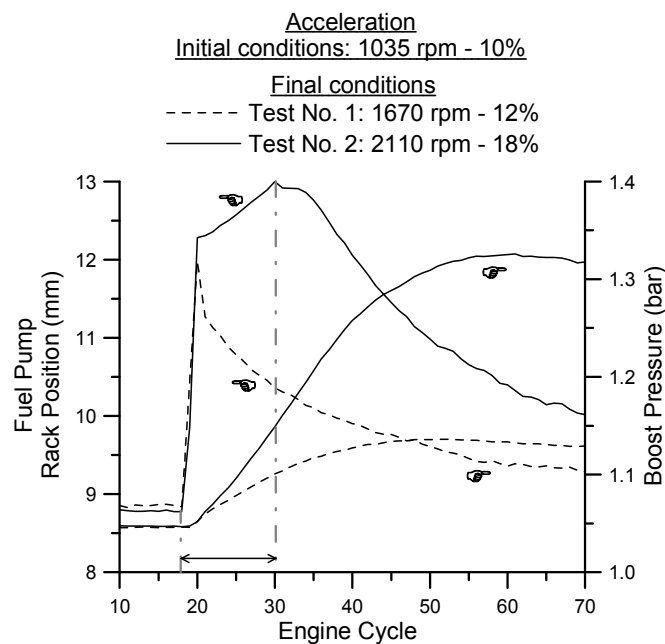


Figure 5. Development of fuel pump rack position and boost pressure response during the accelerations of Figure 4

As it has long been established, turbocharger lag is the most notable off-design feature of diesel engine transient operation that significantly differentiates the torque pattern from the respective steady-state conditions. It happens because, although the fuel pump responds rapidly to the increased fueling demand after a speed (or load) increase, the turbocharger compressor air-supply cannot match this higher fuel-flow instantly, but only

after a number of engine cycles owing to the (flow, mechanical and thermal) inertia of the whole system as there is no mechanical connection between engine crankshaft and turbocharger shaft. The above phenomenon is enhanced by the unfavorable turbocharger compressor characteristics at low loads and speeds (boost pressure depending strongly on turbocharger rotational speed). As a result of this slow reaction, the relative air–fuel ratio during the early cycles of the acceleration assumes very low values (even lower than stoichiometric), deteriorating combustion and leading to slow engine (torque and speed) response and long recovery period [3].

This mismatch between fueling and air-supply has a direct impact on the soot emission profile too, leading to very high opacity values and relatively prolonged black smoke duration until a much lower value is reached after the turbocharger has accelerated to its final operating point. This is identified more clearly in Figure 6, which focuses on opacity development during the first cycles of the transient event, where the above-mentioned phenomena are prominent. For the overshoot in smoke emissions observed, therefore, in Figure 6 during the speed increase, the main cause is the instantaneous lack of air due to turbocharger lag; it has been argued [3,5] that the latter phenomenon is also aided by the initial sharp increase in ignition delay during the early transient cycles of the acceleration. Rapid increases in fuel injection pressure upon the onset of each instantaneous transient cause the penetration of the liquid fuel jet within the combustion chamber to increase. Since the initial higher-pressure fuel jets are injected into an air environment that is practically unchanged from the previous steady-state conditions, the higher-momentum fuel jet is not accompanied by equally enhanced gas motion. Thus, liquid fuel impingement on the cool combustion walls increases, lowering the rate of mixture preparation and enhancing the heterogeneity of the mixture. Moreover, the subsequent harder combustion course prolongs combustion and reduces the available time for soot oxidation.

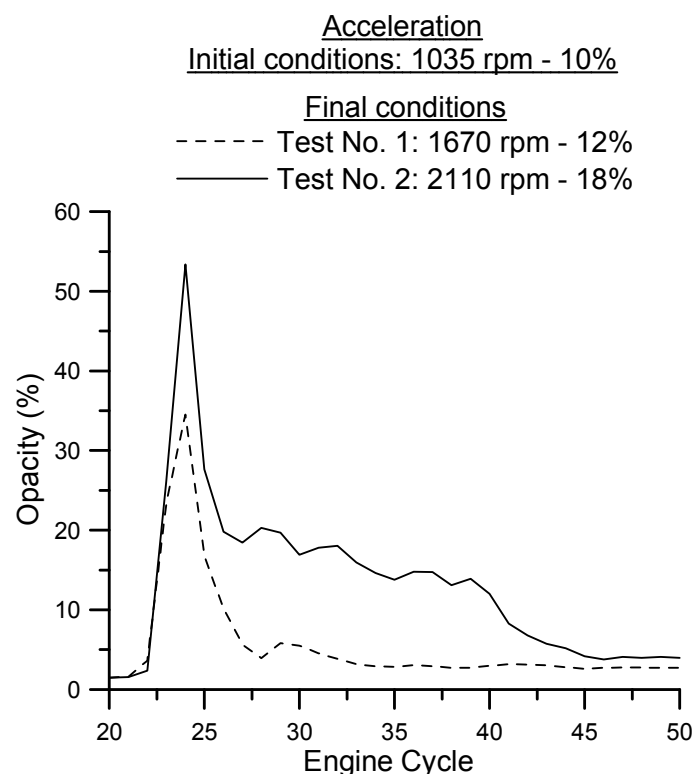


Figure 6. Closer view of opacity emissions during the accelerations of Figure 4

Particularly for test No. 2, the above-mentioned mismatch between fueling and air-supply is even more prominent (it lasts longer too) owing to the harder acceleration schedule compared with test No. 1;

consequently, an extended period of high opacity values, as well as higher cumulative soot emission values are experienced. However, it should be pointed out that for acceleration from higher engine speeds or from higher loads (i.e., with higher gear selected in the gearbox), the smoke overshoot would not be so dramatic, since the turbocharger would accelerate from a higher initial operating point of sufficient boost.

NO concentration is also strongly influenced by the lag between increased fueling and the response of the air-charging system discussed previously, resulting in increased emissions (Figure 4). Since the main parameter affecting NO formation is the burned gas temperature, local high temperatures due to close to stoichiometric air–fuel mixtures (formed because of the still low air-supply) are expected to increase NO during the turbocharger lag cycles. The well-known dependence of NO formation on gas temperature can be documented in Figure 4 by the similarity in the development histories between NO and maximum cylinder pressure; the short (initial) delay observed between these two profiles is unavoidable due to the distance the exhaust gas has to travel until the measurement point is reached which is located downstream of the turbocharger, Figure 1. Especially in test No. 2, there are two NO peaks before stabilizing to its final steady-state value. This is directly related to the respective peaks of maximum cylinder pressure (Figure 4), which in turn are also reflected in gas temperature peaks. The observed NO and smoke emission spikes during such individual transient events have a substantial impact on overall emissions during a Transient Cycle as recently investigated by the present research group regarding the European Light-duty Driving Cycle (EUDC) [39].

The final emission studied is combustion noise, which is closely related to cylinder pressure [40]. In fact, as discussed earlier, its measuring principle is based on the processing of the measured indicator diagrams. In both test cases illustrated in Figure 4, combustion noise emission seems to develop in accordance to the maximum cylinder pressure profile. However, this is not exactly the case, since combustion noise is primarily influenced by the rate of cylinder pressure development (i.e. its gradient with respect to crank angle) during the engine cycle [41]. This rate is affected by various parameters, including injection timing and ignition delay. Particularly, the ignition delay effect is most influential, by assuming higher values during the transient event (especially during the turbocharger lag cycles), owing to the combination of increased fueling with the still low cylinder wall temperatures as the thermal transient develops much slower because of the thermal inertia of the cylinder wall and coolant system [3,42].

Figure 7 investigates the effect of initial loading on the engine acceleration profile. Here, two tests (similar in terms of engine speed accelerations) were performed, differing only in the initial engine loading (representing the gear engaged in vehicular applications). One low and one medium initial load were tried, with the final load affected accordingly; the rate of the pedal change was maintained (almost) the same for both cases.

One of the most influential parameters in Figure 7 is the initial turbocharger operating point, which affects the development of all interesting parameters. Obvious differences are observed between these two cases for all examined variables, with the most remarkable one being the development of combustion noise. Unlike all the other cases discussed previously, combustion noise shows a decreasing trend for the case of acceleration test No. 4 (the one commencing from the medium load and resulting in a high final load). However, it should be noted that the maximum and minimum absolute values during test No. 4 did not differ by more than 3.5 dB. The above trend suggests a reduced rate of cylinder pressure rise (i.e., decreasing 1st derivative of cylinder pressure) throughout the transient event, aided by injection timing retard and shorter ignition delay period. Indeed, these remarks can be documented with reference to Figure 8, where the maximum values of the cylinder pressure gradient and the indicator diagrams of two intermediate cycles of acceleration test No. 4 are presented. As the acceleration develops and engine speed (and loading) increases, the fuel is injected later in the compression stroke, in an environment of higher pressure and temperature resulting in faster ignition. Recall from Table 1 that the static injection timing of the engine is very close to TDC. The synergistic effect of the above two

factors produces a shorter premixed combustion phase at the 46th cycle compared with the 15th, resulting in lower rate of cylinder pressure increase. It is interesting to note that the start of combustion may even move after the ‘hot’ TDC, causing a further significant decrease in the pressure increase rate during compression. Thus, combustion noise decreases as the medium loading acceleration develops.

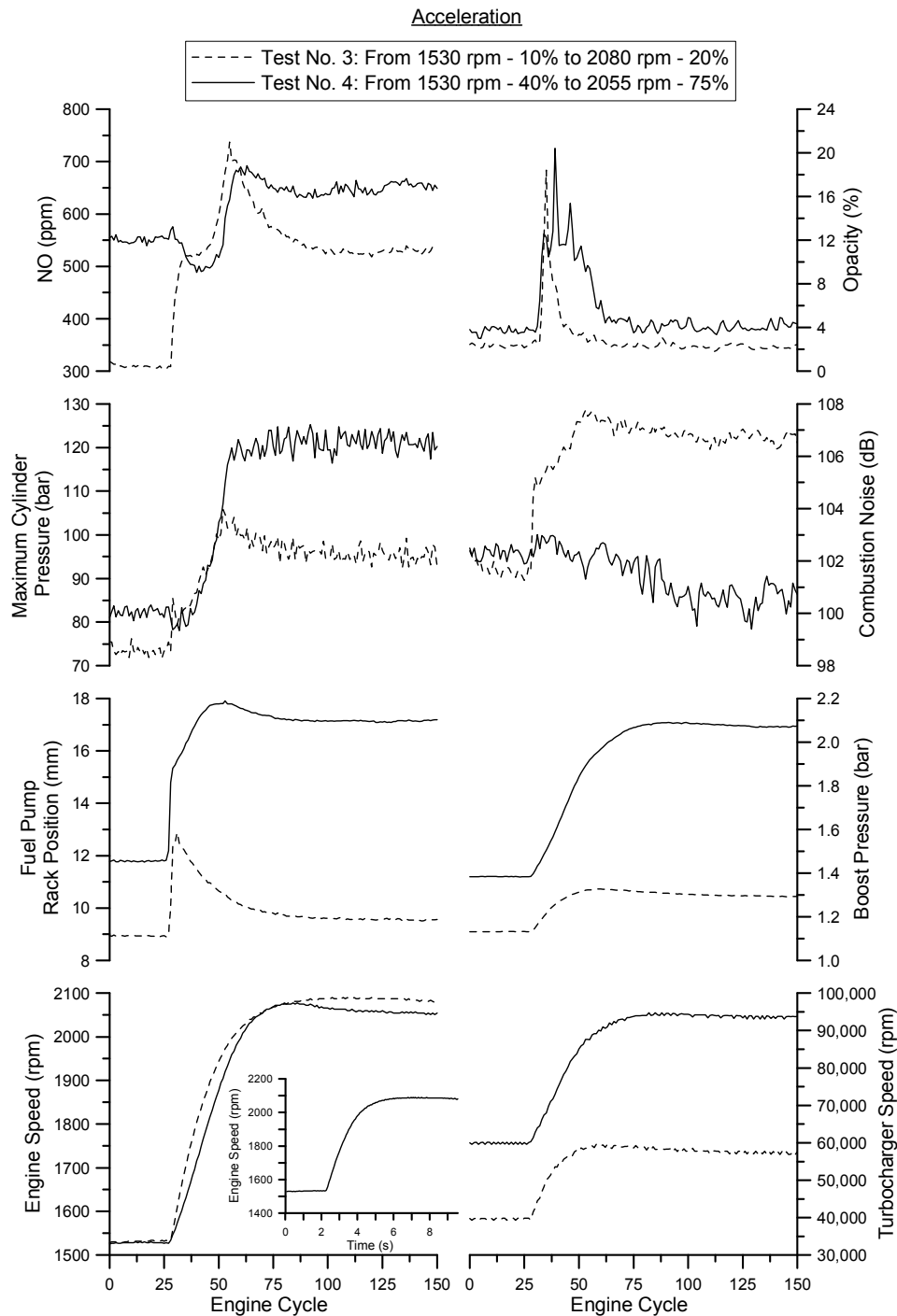


Figure 7. Development of engine and turbocharger variables and emissions response during the acceleration tests No. 3 and 4 (small figure inside engine speed subdiagram illustrates the development with respect to time)

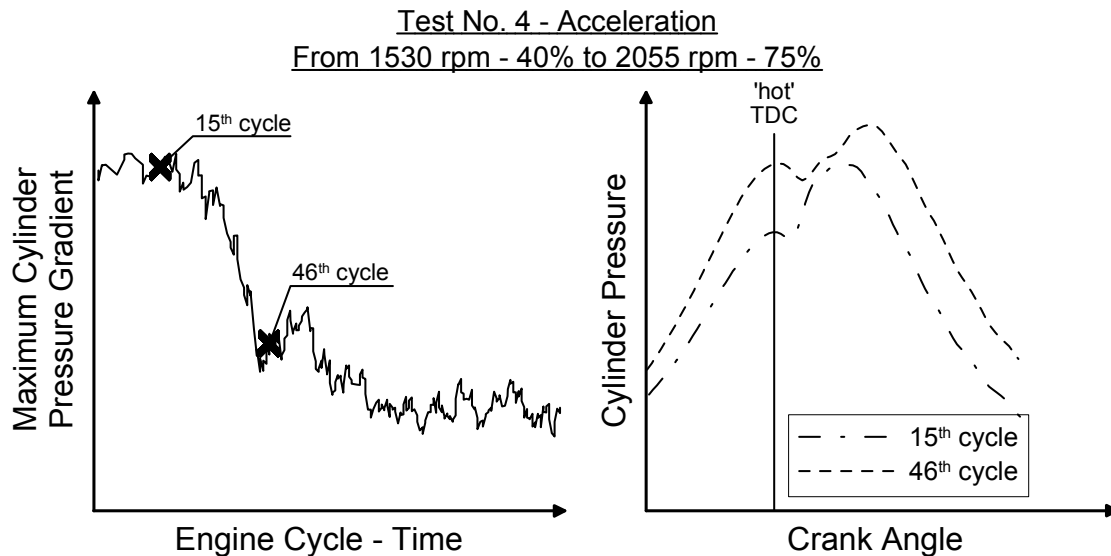


Figure 8. Cylinder pressure diagrams for two cycles of the acceleration test No. 4 of Figure 7

The development of NO emission further supports the previous observations. Although engine load in test No. 4 is considerably higher than in test No. 3, NO peak emission values are comparable. This can be attributed to the shorter premixed combustion phase discussed previously. In fact, the injection calibration of the engine (late injection timing) was chosen exactly for this reason, i.e., limiting of NO emissions at medium-high loads.

Finally, as far as smoke emission is concerned, opacity assumes slightly higher peak values when the acceleration begins from the medium load (test No. 4) due to the overall higher fuel-air equivalence ratio, with the stabilization time to the final steady-state value being considerably longer.

Another important finding from Figure 7 is that although the final engine load for test No. 4 was considerably higher than for test No. 3 (resulting, as expected, in higher final values for both NO and smoke), the peak in soot and NO emissions is practically the same. Recall from the analysis of Figure 4 that the turbocharger lag phenomenon is adversely influenced by the unfavorable turbocharger compressor characteristics at low speeds. For test No. 3, the initial turbocharger speed/boost were minimal, whereas for test No. 4 things were quite better, since the turbocharger was called to accelerate from a considerably higher rotational speed and boost pressure, a fact that limited the extent of both the turbocharger lag phase and the peak in NO and smoke emissions.

LOAD CHANGE TEST RESULTS

The second class of transient operation investigated is the load increase transient event (test No. 5 in Table 2 and Figure 3), the results of which are shown in Figure 9. In general, although automotive engines actually do encounter load change transients, for example when a vehicle climbs a hill, or when engaging the clutch after a gear change, these are not so pronounced as the ones experienced by industrial or marine engines. A significant factor that determines the engine speed response here is the governor operating curves. For the case demonstrated in Figure 9, a rather slow movement of the brake control lever was initiated towards the direction of increased loading (it is worth remembering that due to the less tight governing of automotive engines compared with industrial ones, severe load changes on an uncontrolled automotive engine test bench may lead to engine stall). Initially, the engine was operating at a high rotational speed and low load. The new higher load

was applied by shifting the brake lever position without changing the engine accelerator pedal position. This caused a large engine speed decrease (of the order of 800 rpm), which determined the whole system response.

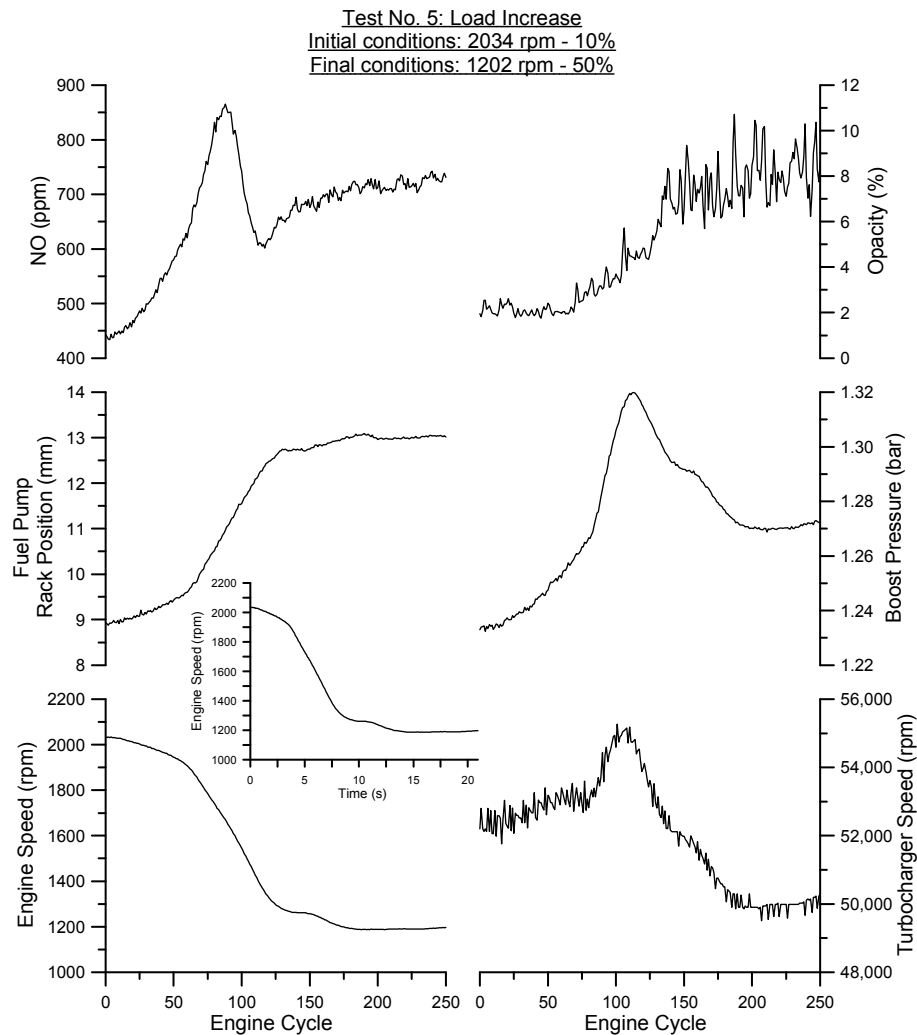


Figure 9. Development of engine and turbocharger variables and emissions response during a load increase transient event (small figure above engine speed subdiagram illustrates the development with respect to time)

During the application of the new higher loading (this lasts for approximately 8 s), the fuel pump governor responds by shifting the rack to a greater fuel delivery position based on the instantaneous speed drop. Following the increase in the applied loading, the engine speed falls at a rather moderate rate (this lasts for approximately 60 cycles), before it decreases sharply and it reaches its final steady-state value almost 170 cycles (approximately 12.9 s) after the beginning of the transient event. Consequently, initially the turbocharger accelerates slowly due to the small increase of exhaust gas energy from the engine originating from the slow rack movement. When the rack manages to achieve an adequately high fuel delivery, the turbocharger accelerates quickly, thus the boost pressure. However, during all this time the engine load has increased at a much lower rate compared with the resistance (brake) load since the governor operating curves are not suited to such intense load increases. Consequently, the engine cannot cope with the load increase, and after approximately 60 cycles the fall in engine speed becomes dominant, initiating a fast decrease of the exhaust gas flow to the turbine and resulting in a sharp reduction of its speed and of the compressor boost pressure.

For NO emission during the load increase, an increasing trend is observed at the beginning owing to the fact that fueling increases at a much higher rate than air-supply, which results in increased fuel–air equivalence ratio and in-cylinder gas temperatures.

On the other hand, the exhaust gas opacity develops initially in a slow manner, but when the fueling rate increases sharply (approx. at cycle No. 60) it exhibits an abrupt increase too, owing to the mismatch between fueling and air-supply. It finally stabilizes at a relatively high value, resulting from the combination of high loading and low engine speed.

ENGINE STARTING TESTS RESULTS

The final class of transient operating schedule investigated is the engine cold and hot starting. The parameter used to identify the starting conditions is the coolant temperature for a fixed idling speed.

Cold Starting

The development of various engine and turbocharger operating parameters and emissions under cold starting is presented in Figure 10. During cold starting, the engine speed is much lower than the required governing speed; hence the fuel pump rack is in the maximum fueling position. Since there is a lack of sufficient air-flow due to the low engine and turbocharger rotational speeds, locally high fuel–air ratios are experienced, leading to flame quenching (owing to shortage of oxygen) and combustion deterioration that may lead to combustion instability between consecutive cycles. As the engine speed gradually increases, the rack moves backwards to lower the fuel supply until it assumes a constant position after the engine has reached its idling speed. It is very important to note here that, even after the engine speed has stabilized, the whole phenomenon continues to develop from the thermal point of view, since a much longer duration is needed for the stabilization of exhaust gas, coolant and lubricating oil temperatures. For example, the gradual heating of the exhaust manifold walls, leads to a decrease of the respective heat losses from the exhaust gases, increasing accordingly the available gas enthalpy at the turbine entry, hence accelerating the turbocharger.

Two remarks concerning engine and turbocharger performance are noteworthy during cold starting. The first is the combustion instability documented by the highly unstable (maximum) cylinder pressure traces illustrated in Figure 10. A more detailed view of the respective indicator diagrams during the first 16 engine cycles is given in Figure 11 that makes clear the previous observation. Cylinder pressure traces show great variation from cycle to cycle, while incomplete combustion and even misfire occur. Three parameters have been identified to be mostly influential for this instability, namely: the low coolant temperature resulting in aggravated heat loss to the cylinder walls, the low oil temperature causing higher frictional losses, as well as the low engine rotational speed allowing more time for the above mentioned two losses to develop and also increasing blow-by losses from the piston rings [3].

The second notable finding during the current cold starting test is the inlet manifold (boost) pressure drop during the first cycles of the transient event. This can also be attributed to turbocharger lag. With reference to Figure 12, during the first four cycles, the turbocharger compressor is not yet rotating; hence the engine sucks the air available in the inlet manifold causing this boost pressure drop. Even after the turbocharger begins to accelerate, it can only reach relatively low rotational speeds (hence boost) owing to the poor energy content of the exhaust gas, primarily originating in the high heat losses to the cylinder and exhaust manifold walls.

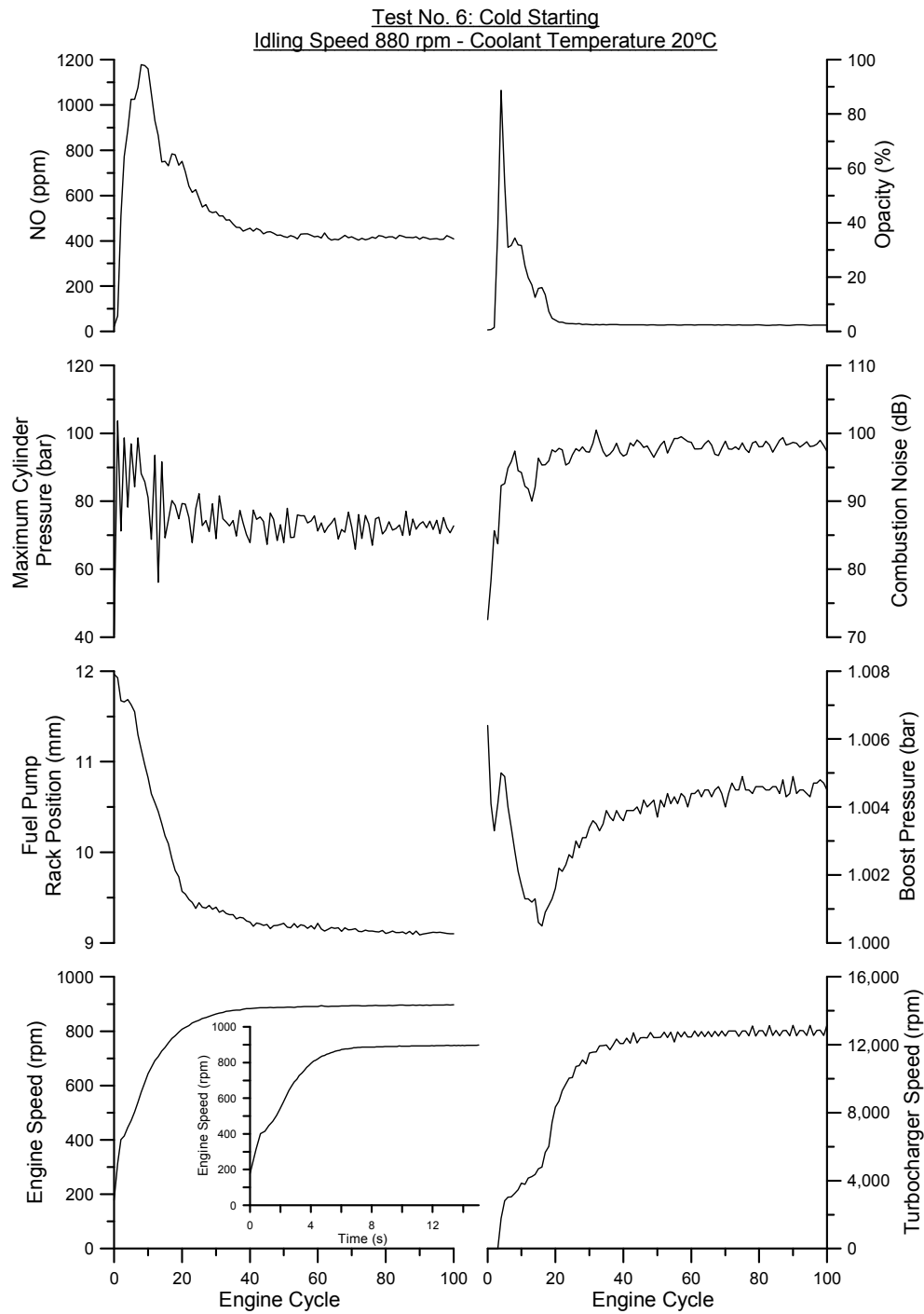


Figure 10. Development of engine and turbocharger variables and emissions response during cold starting (small figure inside engine speed subdiagram illustrates the development with respect to time)

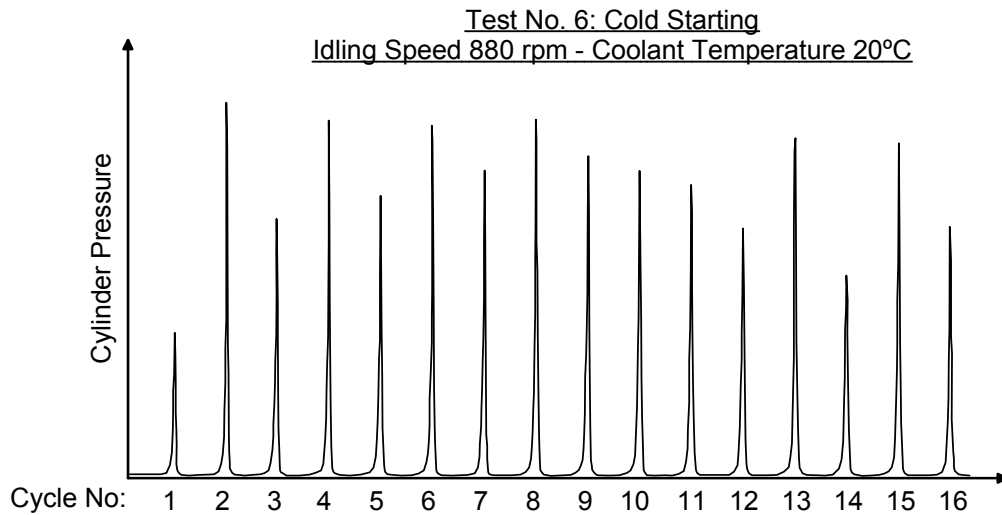


Figure 11. Combustion instability during the cold starting test of Figure 10

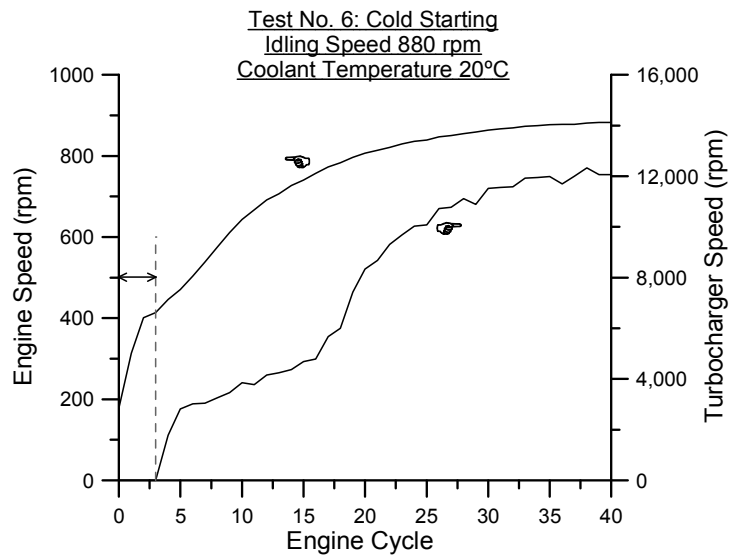


Figure 12. Closer view of engine and turbocharger speed development during the first cycles of the cold starting event of Figure 10

Unsurprisingly, a direct impact of the above-mentioned phenomena on pollutant (mainly) and combustion noise emissions is experienced. Excessive black smoke is noticed coming out from the exhaust pipe, identified by the extremely high values of exhaust gas opacity (reaching almost 100%, Figure 10). The combination of high fueling during cranking with the practically atmospheric inlet manifold pressure is the evident reason. As soon as combustion becomes stable (after almost 30 cycles or 6.2 s) and the engine speed reaches or exceeds the governing self-sustained speed, the rack moves towards the direction of reduced fueling, with a subsequent decrease of smoke emission; the latter is strongly influenced by the coolant temperature. The lower the ambient/coolant temperature, the higher the heat loss to the cylinder walls resulting in lower charge temperature, longer ignition delay and more prolonged period of increased smoke emissions until the engine is warmed-up. It must be noted here that the total smoke emission during (cold and hot) starting may include a portion of soot particles deposited on engine exhaust pipe during the last engine operation. A preconditioning procedure has been suggested in order to reduce this effect [43,44].

NO emission exhibits a relatively high peak value during the first cranking cycles too, before slowly reducing to its final value (not for several cycles owing to the development of the thermal transient discussed earlier). It is a common belief that owing to the low gas temperatures involved during cold starting, NO emissions are, in general, of secondary importance [45,46]. In order to analyze the trend shown in Figure 10 various parameters' effects should be taken into account. On the one hand, the great heat loss to the cylinder walls (low gas temperatures) as well as the very low boost pressures (low oxygen availability) cause little NO to be formed inside the cylinder. On the other hand, the increase of the ignition delay period combined with injection timing advance and the high values of fuel–air equivalence ratio (near stoichiometry) are well known to promote NO production. Past research has suggested that, in certain circumstances, the latter mechanism might become dominant [47], causing an increasing trend of NO with lowering (ambient) temperature. In any case, it is important here to take into account the units used for NO quantification; the volumetric concentration (ppm) used actually assumes higher values the lower the engine rotational speed, thus leading to erroneous interpretations [48] because air mass is not suitably integrated with the ppm values. Furthermore, during cold starting, the air-supply is low due to the very low boost pressure, resulting in high concentration values when the mass of NO is reduced to the total exhaust gas mass.

For the combustion noise trend during cold starting in Figure 10 things are quite obvious. Recall that the main mechanism of combustion noise radiation during a speed (or load) increase comes as the combination of increased fueling with the still low cylinder wall temperature and 'cooled' charge-air temperature. These lead to longer ignition delay, hence more intense premixed combustion period leading to steeper cylinder pressure gradients and, consequently, higher combustion noise levels. The above phenomena are even more prominent during cold starting, where the much lower cylinder wall temperatures lead to even longer ignition delay periods, prolonged premixed combustion phase, hence higher noise emissions. At the 14th cycle where, as seen from Figure 11, a misfire occurred, combustion noise exhibits, as expected, a somewhat lower value.

Hot Starting

Finally, a hot starting event is illustrated in Figure 13. Here the coolant temperature corresponds to fully warmed-up conditions. Although the starting speed is slightly different from the case of cold starting of Figure 10, the results can still be considered comparable. The first important finding is the fuel pump rack final position; for the case of hot starting, the rack stabilizes to a lower fueling position. A contributing factor to this is the higher lubricating oil temperature resulting in much lower frictional losses. Moreover, the turbocharger speed develops much faster now, owing to the greater enthalpy of the exhaust gas. This is directly reflected in the boost pressure, which assumes values relatively higher than atmospheric, with the initial pressure drop being of a much lesser extent compared with the cold starting case. Combustion appears to be more stable, without any misfire detected during the cranking cycles.

As was the case with cold starting, however, emissions are strongly affected. Black smoke assumes excessive values again but the smoky period lasts for a shorter period and the peak opacity values are lower (almost half) than those of the cold starting. Again, the underlying mechanism is the mismatch between fueling and air-supply caused by turbocharger lag. Concerning NO emission, the higher cylinder wall temperatures as well as the relative oxygen availability (owing to higher boost pressures) favor NO formation, while the shorter ignition delay and the lower turbocharger lag effect act against it. The synergistic effect of the above produces NO values that are lower than during the cold starting test. Finally, combustion noise is slightly lower compared to that of cold starting (but still higher than during steady-state conditions), suggesting smaller cylinder pressure gradient, a fact that was expected since both the cylinder wall and the coolant and oil temperatures are higher now.

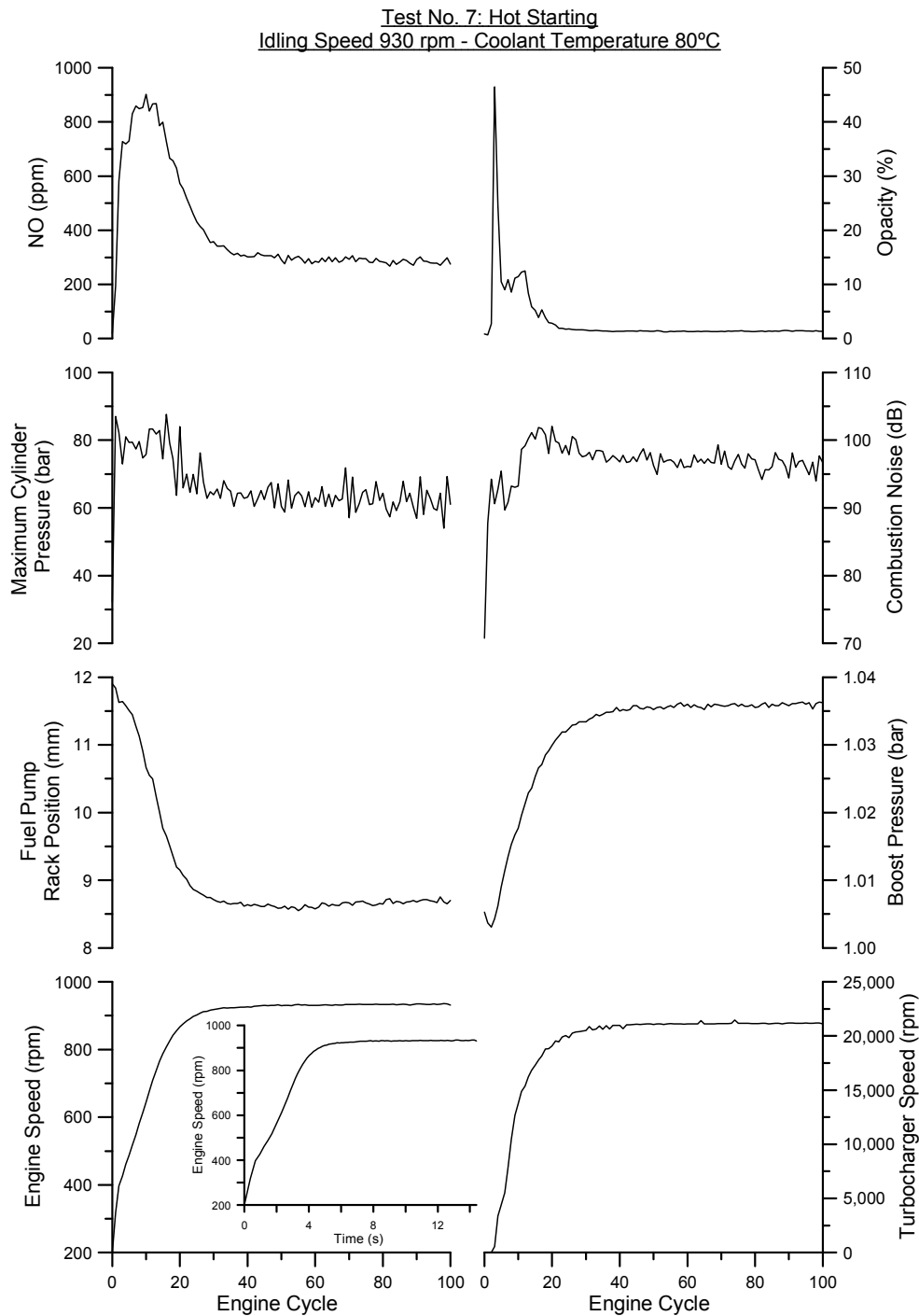


Figure 13. Development of engine and turbocharger variables and emissions response during hot starting (small figure inside engine speed subdiagram illustrates the development with respect to time)

SUMMARY OF RESULTS AND CONCLUSIONS

A fully instrumented test bed installation has been developed in order to study the transient performance and emissions of a medium-duty, turbocharged and after-cooled diesel engine. Fast response analyzers were employed for measuring nitric oxide, smoke opacity and combustion noise emissions. An extended series of

transient tests was performed including various cases of engine acceleration, as well as load increase and starting events. Some of the conclusions derived from the current study, for the specific engine-hydraulic brake configuration, are summarized below:

- As expected, turbocharger lag was found to be the most notable contributor for all transient schedules examined, and the major cause for high values of NO, smoke and combustion noise emissions.
- Fuel limiter action, governing, turbocharger characteristics, engine injection timing calibration and individual specifications of each transient test were found to affect strongly the speed response and the profile and cumulative values of all pollutant emissions.
- A harder or steeper acceleration results in elevated pollutant emissions and prolonged duration until the stabilization to the final value. For accelerations commencing from higher initial loadings a more prolonged smoky period is experienced.
- Combustion noise is directly influenced by the in-cylinder pressure gradient, and may be affected by the specific engine calibration (for the particular engine this consists of retarded injection timing for NO emission limitation).
- A qualitative correlation between combustion noise and NO emission was revealed, but this may be an individual characteristic of the particular engine due to its calibration as mentioned above.
- Load increases of an automotive engine on an uncontrolled brake are strongly influenced by the 'loose' governing, leading to considerable speed drops (even engine stall might occur) and so affecting accordingly the development of all engine and turbocharger parameters and pollutant emissions.
- Combustion instability, excessive black smoke and increased combustion noise radiation are the main characteristics of cold starting. High opacity values (though of smaller magnitude) are also observed under hot starting.

It is believed that the present study has shed more light into the underlying complex phenomena experienced during engine transient operation and particularly as regards NO, smoke and combustion noise radiation development. It is intended to form a basis for deeper research into this challenging field, extending to the investigation of combined transient events and legislated Transient Cycles.

REFERENCES

1. European Automobile Manufacturers' Association (ACEA), <http://www.acea.be>.
2. JD Power and Associates, <http://www.jdpower.com>.
3. Rakopoulos, C. D. and Giakoumis, E. G., Diesel Engine Transient Operation, Springer, London, ISBN 978-1-84882-374-7, 2009.
4. Wijetunge, R. S., Brace, C. J., Hawley, J. G., Vaughan, N. D., Horrocks, R. W., Bird, G. L., "Dynamic Behavior of a High Speed Direct Injection Diesel Engine", SAE Technical Paper 1999-01-0829, 1999.
5. Hagen, J. R., Filipi, Z. S., Assanis, D. N., "Transient Diesel Emissions: Analysis of Engine Operation during a Tip-In", SAE Technical Paper 2006-01-1151, 2006.
6. Rakopoulos, C. D., Giakoumis, E. G., "Review of Thermodynamic Diesel Engine Simulation under Transient Operating Conditions", SAE Technical Paper 2006-01-0884, 2006.
7. Gullett, B. K.; Touati, A.; Oudejans, L.; Ryan, S. P., "Real-Time Emissions Characterization of Organic Air Toxic Pollutants during Steady State and Transient Operation of a Medium Duty Diesel Engine", *Atmos. Environ.* **40**:4037-4047, 2006, [doi:10.1016/j.atmosenv.2006.03.031](https://doi.org/10.1016/j.atmosenv.2006.03.031).
8. <http://ec.europa.eu/enterprise/automotive/directives/vehicles/index.htm>.
9. <http://www.epa.gov/nvfe/testing/dynamometer.htm#engcycles>.
10. Winterbone, D. E., Benson, R. S., Mortimer, A. G., Kenyon, P., Stotter, A., "Transient Response of Turbocharged Diesel Engines", SAE Technical Paper 770122, 1977.

11. Watson, N., "Eliminating Rating Effects on Turbocharged Diesel Engine Response", SAE Technical Paper 840134, 1984.
12. Harndorf, H., and Kuhnt H. W., "Improvement of Transient Behavior of Turbocharged Diesel Engines through Additional Air Injection in the Turbocharger", *MTZ* **56**:20-28, 1995 (in German).
13. Holmén, B. A.; Qu, Y., "Uncertainty in Particle Number Modal Analysis during Transient Operation of Compressed Natural Gas, Diesel and Trap-Equipped Diesel Transit Buses", *Environ. Sci. and Technol.* **38**:2413–2423, 2004, [doi:10.1021/es034560k](https://doi.org/10.1021/es034560k).
14. Winterbone, D. E., "Chapter 20: Transient Performance", in *The Thermodynamics and Gas Dynamics of Internal Combustion Engines*, Vol. II edited by J.H. Horlock and D.E. Winterbone, Clarendon Press, Oxford, ISBN 0-19-856217-8, 1986.
15. Watson, N. and Janota, M. S., *Turbocharging the Internal Combustion Engine*, MacMillan, London, ISBN 0-333-24290-4, 1982.
16. Kang, H., Farrell, P. V., "Experimental Investigation of Transient Emissions (HC and NO_x) in a High Speed Direct Injection (HSDI) Diesel Engine", SAE Technical Paper 2005-01-3883, 2005.
17. Black, J., Eastwood, P. G., Tufail, K., Winstanley, T., Hardalupas, Y., Taylor, A. M. K. P., "Diesel Engine Transient Control and Emissions Response during a European Extra-Urban Drive Cycle (EUDC)", SAE Technical Paper 2007-01-1938, 2007.
18. Campbell, B., Peckham, M., Symonds, J., Parkinson, J., Finch, A., "Transient Gaseous and Particulate Emissions Measurements on a Diesel Passenger Car Including a DPF Regeneration Event", SAE Technical Paper 2006-01-1079, 2006.
19. Armas, O., Cardenas, M. D., Mata, C., "Smoke Opacity and NO_x Emissions from a Bioethanol-Diesel Blend during Engine Transient Operation", SAE Technical Paper 2007-24-0131, 2007.
20. Bazari, Z., "Diesel Exhaust Emissions Prediction under Transient Operating Conditions", SAE Technical Paper 940666, 1994.
21. Chan, S. H.; He, Y.; Sun, J. H., "Prediction of Transient Nitric Oxides in Diesel Exhaust", *Proceedings of the Institution of Mechanical Engineers, Part D: J. of Autom. Eng.* **213**:327-339, 1999, [doi:10.1243/0954407991526892](https://doi.org/10.1243/0954407991526892).
22. Rakopoulos, C. D., Dimaratos, A. M., Giakoumis, E. G., and Rakopoulos D. C., "Exhaust Emissions Estimation during Transient Turbocharged Diesel Engine Operation Using a Two-Zone Combustion Model", *Int. J. of Veh. Des.* **49**(1/2/3):125-149, 2009.
23. Giakoumis, E. G.; Alafouzos, A. I., "Study of Diesel Engine Performance and Emissions during a Transient Cycle Applying an Engine Mapping-Based Methodology", *Appl. Energy* **87**:1358-1365, 2010, [doi:10.1016/j.apenergy.2009.09.003](https://doi.org/10.1016/j.apenergy.2009.09.003).
24. Ericson, C., Westerberg, B., Egnell, R., "Transient Emission Predictions with Quasi Stationary Models", SAE Technical Paper 2005-01-3852, 2005.
25. McClure, B. T., "Characterization of the Transient Response of a Diesel Exhaust-Gas Measurement System", SAE Technical Paper 881320, 1988.
26. Beaumont, A. J., Noble, A. D., Pilley, A. D., "Signal Reconstruction Techniques for Improved Measurement of Transient Emissions", SAE Technical Paper 900233, 1990.
27. Chan, S. H., Chen, X. S., and Arcoumanis, C., "Measurement and Signal Reconstruction of Transient Nitric Oxide Emissions in the Exhaust of a Turbocharged Diesel Engine", *Transactions of the ASME, J. of Dynam. Sys., Meas. and Contr.* **119**:620-630, 1997.
28. Wachter, W. F., "Analysis of Transient Emissions Data of a Model Year 1991 Heavy Duty Diesel Engine", SAE Technical Paper 900443, 1990.
29. Bielaczyc, P., Merkisz, J., Pielecha, J., "Investigation of Exhaust Emissions from DI Diesel Engine during Cold and Warm Start", SAE Technical Paper 2001-01-1260, 2001.
30. Arcoumanis, C., Yao, X. G., "Transient Smoke and Unburnt Hydrocarbon Emissions during Cold-Start in a Turbocharged DI Diesel Engine", SAE Technical Paper 944122, 1994.

31. "Commission Directive 96/20/EC of 27 March 1996 adapting to technical progress Council Directive 70/157/EEC relating to the permissible sound level and the exhaust system of motor vehicles", Official Journal L 092, April 1996.
32. Dhaenens, M., van der Linden, G., Nehl, J., Thiele, R., "Analysis of Transient Noise Behavior of a Truck Diesel Engine", SAE Technical Paper 2001-01-1566, 2001.
33. Alt, N., Sonntag, H. D., Heuer, S., Thiele, R., "Diesel Engine Cold Start Noise Improvement", SAE Technical Paper 2005-01-2490, 2005.
34. Cambustion Ltd., Cambridge, UK, <http://www.cambustion.co.uk>.
35. CLD500 Fast NO_x Measurement System, User Manual (version 2.2), Cambustion Ltd., 2008.
36. Collier, T., Gregory, D., Rushton, M., Hands, T., "Investigation into the Performance of an Ultra-Fast Response NO Analyzer Equipped with a NO₂ to NO Converter for Gasoline and Diesel Exhaust NO_x Measurements", SAE Technical Paper 2000-01-2954, 2000.
37. AVL 439 Opacimeter, Operating Manual, AVL, November 2006.
38. AVL 450 Combustion Noise Meter, Operating Manual, AVL, August 2000.
39. Giakoumis, E.G., and Lioutas, S.C., "Estimation of Diesel-Engined Vehicle Nitric Oxide and Soot Emissions during the European Light-Duty Driving Cycle Based on a Transient Mapping Approach", *Transportation Research, Part D: Transport. and Environment*, 2010 (in press).
40. Taylor, C. F., The Internal Combustion Engine in Theory and Practice, Vol. 2, MIT Press, Cambridge, MA, ISBN 0-262-70027-1, 1985.
41. Zhao, H. and Ladamatos, N., Engine Combustion Instrumentation and Diagnostics, SAE Inc., Warrendale, Pennsylvania, ISBN 0-7680-0665-1, 2001.
42. Rust, A., Thien, G. E., "Effect of Transient Conditions on Combustion Noise of NA-DI Diesel Engines", SAE Technical Paper 870989, 1987.
43. Arregle, J.; Bermúdez, V.; Serrano, J.R.; Fuentes, E., "Procedure for engine transient cycle emissions testing in real time", *Exp. Thermal and Fluid Sci.* **30**:485-496, 2006, [doi:10.1016/j.expthermflusci.2005.10.002](https://doi.org/10.1016/j.expthermflusci.2005.10.002).
44. Andrews, G.E., Clarke, A.G., Rojas, N.Y., "The Transient Storage and Blow-Out of Diesel Particulate in Practical Exhaust Systems", SAE Technical Paper 2001-01-0204, 2001.
45. Broatch, A.; Luján, J. M.; Ruiz, S.; Olmeda, P., "Measurement of Hydrocarbon and Carbon Monoxide Emissions during the Starting of Automotive DI Diesel Engines", *Int. J. of Autom. Technol.* **9**(2):129-140, 2008, [doi:10.1007/s12239-008-0017-6](https://doi.org/10.1007/s12239-008-0017-6).
46. Heywood, J. B., Internal Combustion Engine Fundamentals, McGraw-Hill, New York, ISBN 0-07-100499-8, 1988.
47. Weilenmann, M.; Favez, J. Y.; Alvarez, R., "Cold-Start Emissions of Modern Passenger Cars at Different Low Ambient Temperatures and their Evolution over Vehicle Legislation Categories", *Atmos. Environ.* **43**:2419-2429, 2009, [doi:10.1016/j.atmosenv.2009.02.005](https://doi.org/10.1016/j.atmosenv.2009.02.005).
48. Grados, C. V. D.; Uriondo, Z.; Clemente, M.; Espadafor, F. J. J.; Gutiérrez, J. M., "Correcting Injection Pressure Maladjustments to Reduce NO_x Emissions by Marine Diesel Engine", *Transp. Res. Part D* **14**:61-66, 2009, [doi:10.1016/j.trd.2008.09.012](https://doi.org/10.1016/j.trd.2008.09.012).

CONTACT INFORMATION

C.D. Rakopoulos (cdrakops@central.ntua.gr), A.M. Dimaratos (adim@mail.ntua.gr), E.G. Giakoumis (vgiakms@central.ntua.gr), Internal Combustion Engines Laboratory, Thermal Engineering Department, School of Mechanical Engineering, National Technical University of Athens, 9 Heroon Polytechniou Str., Zografou Campus, 15780, Athens, Greece; M.S. Peckham (msp@cambustion.com), Cambustion Ltd., 347 Cherry Hinton Road, Cambridge, CB1 8DH, UK.

ACKNOWLEDGMENT

The authors would like to thank Turbo Hellas Trading Ltd. for the donation of the turbocharger speed sensor kit.

DEFINITIONS/ABBREVIATIONS

°CA	degrees crank angle
BDC	bottom dead center
dB	decibels
NO	nitric oxide
NO ₂	nitrogen dioxide
NO _x	nitrogen oxides
ppm	parts per million
rpm	revolutions per minute
TDC	top dead center